https://doi.org/10.5194/tc-2022-244
Preprint. Discussion started: 8 December 2022

The Cryosphere
Discussions
Open Access
EGU

Change in the potential snowfall phenology: past, present, and future in the Chinese Tianshan mountainous region, Central Asia

Xuemei Li[1,2,3], Xinyu Liu[1,2,3], Kaixin Zhao[1,2,3], and Lanhai Li[4,5]

[1]Faculty of Geomatics, Lanzhou Jiaotong University, Lanzhou 730070, China;
[2]National-Local Joint Engineering Research Center of Technologies and Applications for National Geographic State Monitoring, Lanzhou 730070, China;
[3]Gansu Provincial Engineering Laboratory for National Geographic State Monitoring, Lanzhou 730070, China;
[4]State Key Laboratory of Desert and Oasis Ecology, Xinjiang Institute of Ecology and Geography, Chinese Academy of Sciences, Urumqi 830011, China;
[5]Research Center for Ecology and Environment of Central Asia，Chinese Academy of Sciences，Urumqi 830011，China

Correspondence: Xuemei Li (lixuemei@mail.lzjtu.cn)

Abstract. Rapid climate warming speeds up the solid-liquid water cycle and reduces the solid water storage in cold regions of the Earth. Snowfall is the most crucial input for the cryosphere. However, the potential snowfall phenology (PSP) variability has not been systematically and comprehensively studied. For this reason, we initially proposed three indicators, i.e., the start of potential snowfall season (SPSS), the end of potential snowfall season (EPSS), and the length of potential snowfall season (LPSS), to describe the characteristics of the PSP, then we explored the spatial-temporal variation of those three PSP indicators past, present, and future across the Chinese Tianshan mountainous region (CTMR) based on the observed daily air temperature from 26 meteorological stations during 1961-2017/2020 combined with 14 models data from CMIP6 (the Phase 6 of the Coupled Model Intercomparison Project) under four different scenarios (SSP126, SSP245, SSP370, and SSP585) during 2021-2100. It proved that the SPSS, EPSS, and LPSS could reproduce features of the PSP well across the study area. In the past and present, the potential snowfall season started on October 29th, ended on March 20th, and lasted for about four months and 23 days across the CTMR on average. The rate of advancing EPSS (-1.6 days/10a) was faster than that of postponing SPSS (1.1 days/10a) during 1961-2017/2020. It also found significant delaying by 2-13 days in the starting time, and advancing for 1-13 days in the ending time, respectively, which reduced 1-27 days for the LPSS. The potential snowfall season started later, ended later, and lasted longer in the north and center than in the south. Similar to the past and present, the SPSS, EPSS, and LPSS will vary under four emission scenarios during 2021-2100. Potential snowfall season will start later, end earlier, and last fewer days under the higher emission scenario. Under the highest emission scenario, SSP585, the starting time will be postponed by 41 days in 2100, while the ending time will be up to 23 days in advance in 2100, implying that it will cut down the length by 63 days (about two months), and the length of the potential snowfall season will only last two and a half months in 2100 under the SSP585 scenario. Spatially, the length of the potential snowfall season in the west and southwest of the CTMR will be compressed by more days because of the more delayed starting time and advanced ending time under all four scenarios. The results indicate that annual total snowfall will decrease, including amount and frequency, then reduce snow cover or mass, which finally feedback to the atmosphere in the form of more rapid warming for the lower reflectivity to solar radiation. Our research provides a new direction to capture the potential snowfall phenology in the alpine region and can be easily

https://doi.org/10.5194/tc-2022-244
Preprint. Discussion started: 8 December 2022

expanded to other snow-dominated areas worldwide.

Keywords: Rapid climate warming, potential snowfall phenology, spatial-temporal variation, Chinese Tianshan mountainous region

1 Introduction

Global glaciers, sea ice, and snow cover decrease, and the growing season lengthen almost everywhere, reflecting global warming in various aspects (Kappelle, 2020). However, rates of climate warming vary in different regions. Generally, the warming rate is more significant in the continent than in the ocean and more significant in the mid-high latitudes than in the tropics (IPCC., 2021). For the high sensitivity of glaciers and snow to climate change and considerable variation of topography in the mountains, mountainous regions are pretty sensitive to increasing temperature and changing precipitation (Dedieu et al., 2014; Piazza et al., 2014; Roux et al., 2021). Hence, mountains are regarded as outposts of global climate change (Sorg et al., 2012; Immerzeel et al., 2020), and the warming rate in the mountains is about twice that of the rest of the planet (Sabine et al., 2022). Although it is estimated that annually 1773 km^3 of snow (about 5% of the global snowfall accumulations) could fall over international mountains on average, rapid climate warming is reducing the proportion of precipitation falling as snow, leading to predicted snow mass reductions of up to 25% over the next 10 to 30 years (Daloz et al., 2020; Hock et al., 2022).

Snowfall is one of the dominant water resources in the mountainous region that invariably influences human society and natural ecosystems with the exchange of energy and water cycles (Krasting, 2008; McAfee et al., 2014; Bai et al., 2019; Zhang et al., 2019; Tamang et al., 2020). In response to recent climate warming, the change happened in snowfall amount and phenology (e.g., the start of the snowfall season, the end of the snowfall season, the length of the snowfall season, etc.). Less snowfall in winter was caused by higher surface temperature due to increased greenhouse gas emissions (Sun et al., 2016). In late winter, the increased occurrence of above-zero temperatures reduces the fraction of snowfall and enhances snow-melting in the mid-winter (Raisanen, 2016). The declining amount of snow caused by increasing temperature was observed in North America, especially in the United States (Hamlet et al., 2005; Mote, 2005; McCabe et al., 2009; Clow, 2010). For the snowfall phenology, postponed snowfall occurrence and advanced snowfall ending took place across the Eurasian continent (Bai et al., 2019; Lin and Chen, 2022).

In the Northern Hemisphere, air temperature within a year obeys a specific pattern, i.e., the air temperature gradually increases from the beginning of a year to the middle of a year and then steadily decreases until the end of a year (Marshall and Plumb, 2008). Precipitation falls on the ground in various phases, such as rainfall, snowfall, and sleet, and each phase has a vital impact on surface runoff and the energy balance (Loth et al., 1993; Wei et al., 2018). When the air temperature reach a threshold, called rain-snow threshold (RST), precipitation falls as rain and snow with equal frequency, while above the threshold precipitation falls primarily as rain and below primarily as snow (Jennings et al., 2018). Thereby, with air temperature below the RST in winter, potential snowfall may occur under the condition that all other conditions (water vapor, air pressure, condensation nodules etc.) are satisfied. Until the air temperature in the next year gradually increases to over the RST, potential snowfall may end. Potential snowfall season could cover the period when the air temperature below the RST within two consecutive years.

The Chinese Tianshan mountainous region (CTMR) is a typical alpine region with high topographic heterogeneity (Li et al., 2022). Regional warming amplification and altitude warming

https://doi.org/10.5194/tc-2022-244
Preprint. Discussion started: 8 December 2022

amplification in the CTMR were detected (Gao et al., 2021). Mean annual snowfall estimated will decrease by 26.5% in 2070-2099 under RCP8.5 in the CTMR (Yang et al., 2017). Snowfall is an indispensable resource and quite sensitive to climate change in the alpine region of Asia (Kapnick et al., 2014). Quantifying changes in potential snowfall phenology (PSP) is essential to enable an improved understanding of present and future climate change allowing the development of adaptation policies. However, few studies have technically focused on the PSP and its variability in the CTMR. Air temperature is the crucial driving factor in the variation of snowfall and the shift from snowfall to rainfall in the CTMR (Zhang et al., 2019; Ren et al., 2020; Ren et al., 2022). The semi-sinusoid curve could fit the intra-annual distribution of air temperature (IADAT) well in Northwestern China, including the CTMR (Li et al., 2015). In addition, RST varies significantly across the Northern Hemisphere, and different precipitation phase discrimination methods showed distinctive RST values (Jennings et al., 2018). In the CTMR, spatially inconsistent RSTs could be obtained based on the frequency intersection method and the probability guarantee method (Zhang et al, 2017). Thus, this paper initially defines three indicators of the PSP combined with the semi-sinusoid curve and RST line firstly, then, the variation of the PSP past, present, and future are explored based on observed data from available meteorological stations in the CTMR and 14 models data from CMIP6 (Phase 6 of the Coupled Model Inter-comparison Project) under four different scenarios. The next section of the paper provides more details on the study area, data, and methods, including the definition of three indicators of the PSP. Then, change in the PSP across the CTMR is evaluated in Section 3. The paper ends with a discussion and conclusions.

2 Study area, data, and methods

2.1 Study area

Located in the heart of the Eurasian continent, Tianshan mountain is most extensive mountain system of Central Asia. Its width and length are approximately 250-350 km and 2500 km, respectively, with an area of 8×10^5 km^2 spanning from Uzbekistan to Kyrgyzstan, southeastern Kazakhstan, and Xinjiang (China) (Aizen et al., 1997; Yang et al., 2019; Li et al., 2020). The CTMR, the part within Xinjiang, China, about 5.7×10^5 km^2 (about 1700 km long), accounts for 34.5% of the total area of Xinjiang Uygur Autonomous Region (Hu, 2004; Li et al., 2020) (Figure 1). The average height of the mountain ridge is 4000 m.a.s.l., with the highest peak being Tomor (7435 m a.s.l.). The CTMR is a typical alpine mountainous area characterized by a continental climate with significant seasonal differences. Mainly affected by the westerly circulation and topography, the CTMR has abundant precipitation and is regarded as the primary source of water resources in Xinjiang. The annual mean air temperature and the annual precipitation are 7.7 ºC and 189.58 mm, respectively (Li et al., 2016; Li et al., 2020). The warming is widespread in the CTMR with an extensive seasonal amplitude of variation (Li et al., 2022). The snowfall in the CTMR mainly occurs from November to February, while rainfall, snowfall, or sleet coexist in March and April. In recent years, both snowfall and rainfall in the CTMR exhibited a significant increasing trend, the growth rate of rainfall is greater than that of snowfall, and S/P (the fraction of snowfall to precipitation) had a significant decreasing trend (Guo and Li, 2015; Zhang et al., 2019). Winter snowfall can reach 84.53 mm with a slight increase (Yang et al., 2022). The frequency of rainfall increases while that of snowfall decreases. Besides, precipitation shifting from solid to liquid is obvious (Tian et al., 2020; Li, 2021).

https://doi.org/10.5194/tc-2022-244
Preprint. Discussion started: 8 December 2022

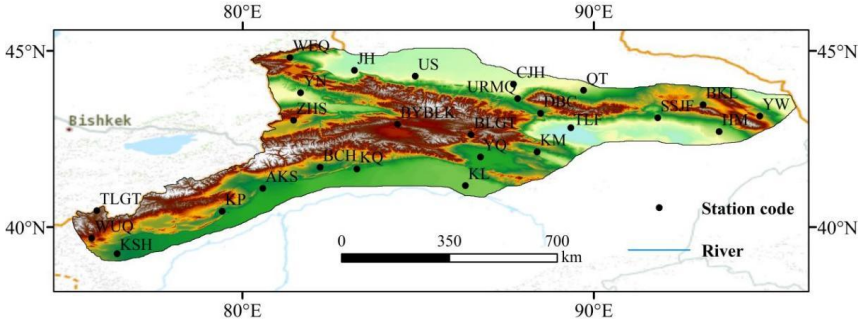

Figure 1. Distribution of the meteorological stations in the CTMR. The full name and descriptive information of all meteorological stations selected can refer to Table 1

2.2 Data

2.2.1 Observed historical daily air temperature data

This study used the observed daily air temperature data covering 1961-2017/2020 from 26 meteorological stations in the CTMR (Figure 1), provided by China Meteorological Data Service Centre (http://data.cma.cn). The data quality was firmly controlled before its release, and homogeneity tests were also performed (Jiang et al., 2009; Li et al., 2015; Li et al., 2020). Then the daily air temperature data were subjected to a quality control procedure, which involved visualizing individual stations or grid records to identify outliers. The identified outliers were either removed or corrected. Only a tiny fraction of the data needed correction. Missing daily values, accounting for less than 2% of the total data, were estimated for a given day by extrapolating the average value of the data from the one or two preceding and following records. It omitted any time series with more than one year of missing data from meteorological stations for this study. Finally, we used daily air temperature data during 1961-2017 from 12 meteorological stations and that during 1961-2020 from 14 meteorological stations across the CTMR. Additionally, The average values of RSTs (also called RST) computed based on the frequency intersection method and the probability guarantee method from the 26 meteorological stations in the CTMR (Zhang et al, 2017) were used as the thresholds to distinguish potential rainfall and snowfall. Table 1 shows the details of the 26 meteorological stations.

https://doi.org/10.5194/tc-2022-244
Preprint. Discussion started: 8 December 2022

The Cryosphere Discussions
Open Access
EGU

Table 1. Descriptive information of meteorological stations selected, including name, code, latitude, longitude, elevation, and RST in the CTMR

No.	Station name	Station code	Latitude (°N)	Longitude (°E)	Elevation (m)	RST(℃)
1	Aksu	AKS	80.23	41.17	1104.73	3.77
2	Baicheng	BCH	81.90	41.78	1230.00	3.35
3	Balguntay	BLGT	86.30	42.73	1739.47	5.59
4	Barkol	BKL	93.05	43.60	1675.37	3.59
5	Bayanbulak	BYBLK	84.15	43.03	2459.27	3.70
6	Caijiahu	CJH	87.53	44.20	440.97	1.80
7	Dabancheng	DBCH	88.32	43.35	1104.77	3.61
8	Hami	HM	93.52	42.82	738.20	3.34
9	Jinghe	JH	82.90	44.60	320.87	1.98
10	Kalpin	KP	79.05	40.50	1162.63	4.24
11	Kashi	KSH	75.99	39.27	1291.20	3.79
12	Korla	KL	86.13	41.25	932.43	2.90
13	Kumux	KM	88.22	42.23	923.47	3.50
14	Kuqa	KQ	82.97	41.73	1082.93	3.56
15	Qitai	QT	89.57	44.02	794.10	2.55
16	Shisanjianfang	SHSJF	91.73	43.22	722.90	3.75
17	Tuergate	TEGT	75.40	40.52	3506.40	4.03
18	Turpan	TP	89.20	42.93	34.97	2.11
19	Urumqi	URMQ	87.65	43.78	935.67	2.24
20	Usu	US	84.67	44.43	478.97	2.33
21	Wenquan	WEQ	81.02	44.97	1358.60	1.47
22	Wuqia	WUQ	75.25	39.72	2176.90	3.67
23	Yining	YN	81.33	43.95	663.20	1.84
24	Yanqi	YQ	86.57	42.08	1056.60	2.27
25	Yiwu	YW	94.70	43.27	1728.60	4.34
26	Zhaosu	ZHS	81.13	43.15	1853.40	2.70

2.2.2 The modeled future daily air temperature data

The Shared Socioeconomic Paths (SSPs) describe social change in the future without climate policy intervention within CMIP6 (O'Neill et al., 2016). The SSP126, SSP245, SSP370, and SSP585 scenarios correspond to the anthropogenic radiative forcing stabilized at 2.6 w/m^2, 4.5 w/m^2, 7.0 w/m^2, and 8.5 w/m^2 in 2100, respectively (Zhang et al., 2019). This paper selected daily air temperature data from 14 models, including ACCESS-ESM1-5, BCC-CSM2-MR, CanESM5, CESM2-WACCM, CMCC-ESM2, CNRM-CM6-1, CNRM-ESM2-1, INM-CM4-8, INM-CM5-0, IPSL-CM6A-LR, MIROC6, MRI-ESM2-0, NorESM2-LM, and NorESM2-MM (Table 2). Those 14 models could provide daily air temperature under the SSP126, SSP245, SSP370, and SSP585 scenarios spanning 2021 to 2100. Since model resolutions were unsuitable for regional change and differed from the horizontal resolution of observation data, the horizontal resolution was

https://doi.org/10.5194/tc-2022-244
Preprint. Discussion started: 8 December 2022


The Cryosphere Discussions
Open Access
EGU

resampled to 0.25°×0.25°. To solve the uncertainty among modes and better compare and analyze the model data with the observation data, we used the multi-model ensemble averaging method and the bilinear interpolation method to interpolate the model data to the meteorological stations across the CTMR. The delta deviation correction method was employed to correct the deviation between the bilinear interpolated, multi-models averaged, and the observed daily temperature data (Li et al., 2021). The period, 2021-2100, was divided into 2021-2040, 2041-2070, and 2071-2100, respectively. Finally, a daily 14-model ensemble averaged air temperature under four scenarios during three periods was used to analyze the future change of PSP indicators in the CTMR.

Table 2. Basic information of 14 models from the CMIP6

No.	Model name	Institution	Country/Region	Resolution (lat×lon)
1	ACCESS-ESM1-5	ACCESS	Australia	145×192
2	BCC-CSM2-MR	BCC	China	320×160
3	CanESM5	CCCma	Canada	128×64
4	CESM2-WACCM	NCAR	America	192×288
5	CMCC-ESM2	CMCC	Italy	256×128
6	CNRM-CM6-1	CNRM-CERFACS	France	256×128
7	CNRM-ESM2-1	CNRM-CERFACS	France	256×128
8	INM-CM4-8	INM	Russia	180×120
9	INM-CM5-0	INM	Russia	180×120
10	IPSL-CM6A-LR	IPSL	France	144×143
11	MIROC6	MIROC	Japan	256×128
12	MRI-ESM2-0	MRI	Japan	160×320
13	NorESM2-LM	NCC	Norway	144×96
14	NorESM2-MM	NCC	Norway	288×192

2.3 Methods

2.3.1 Definition of PSP indicators

The semi-sinusoidal curve can fit the intra-annual distribution of 10-day air temperature very well across Northwestern China (Li et al., 2015). Here we used the same equation to describe the intra-annual distribution of daily mean air temperature for a site. The semi-sinusoidal curve function, EPSS, SPSS, and LPSS for a site were shown as follows:

$$T_i = A_i \sin(w_i t + \varphi_i) \quad (1)$$

$$EPSS_i = (\arcsin(RST/A_i) - \varphi_i)/w_i \quad (2)$$

$$SPSS_i = (\pi - \arcsin(RST/A_i) - \varphi_i)/w_i \quad (3)$$

$$LPSS_{i\rightarrow(i+1)} = 365 + EPSS_{i+1} - SPSS_i \quad (4)$$

where i represents the year (i=1961, 1962, 1963,…, 2100) and t represents the day of Julian's year (DOY, t=1, 2, 3,…, 365 or 366). T_i is the simulated daily mean air temperature time series of the i^{th} year based on the semi-sinusoidal curve function. A_i, ω_i, and φ_i are shape parameters of the semi-sinusoidal curve estimated by the nonlinear least-squares method. RST is the rain-snow threshold. Two intersection points exist between the fitting curve and RST line. $EPSS_i$ stands for the left intersection point, and $SPSS_i$ for the right within the i^{th} year for a site. Similarly, $EPSS_{i+1}$ stands for the left intersection point, and $SPSS_{i+1}$ for the right within the $(i+1)^{th}$ year for a site (Figure 2). In addition, $LPSS_{i\rightarrow(i+1)}$ represents the horizontal distance from $SPSS_i$ to $EPSS_{i+1}$ and can be calculated by equation (4). Therefore, if the SPSS and EPSS are from 1961 to 2017/2020, while the LPSS is from 1962 to 2017/2020 for a site.

https://doi.org/10.5194/tc-2022-244
Preprint. Discussion started: 8 December 2022

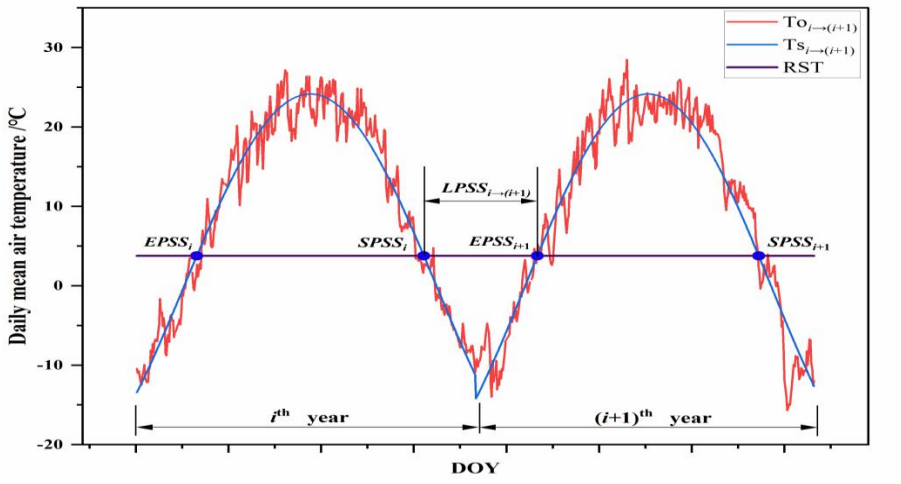

Figure 2. The fitting curve, the observed curve of daily mean air temperature within two consecutive years (the i^{th} year and the $(i+1)^{th}$ year), and three PSP indicators for a location in the CTMR. EPSS, the end of the potential snowfall season; SPSS, the start of the potential snowfall season; LPSS, the length of the potential snowfall season.

2.3.2 Mann-Kendall monotonic test method

The non-parametric Mann-Kendall (M-K) test method has the advantages of not requiring data to follow a specific distribution and being less sensitive to outliers and missed values (Kendall, 1990). This method is widely applied for detecting the significance of long-term trends in a time series from hydrology and climatology, such as temperature, precipitation, and runoff (Li et al., 2011; Li et al., 2022). Specific information about this method can refer to Kendall (1990) and Li et al. (2011). This paper employed the M-K test method to test the changing trends of PSP indicators across the study area.

3 Results

3.1 General characteristic of PSP indicators past and present

Three PSP indicators, the SPSS, the EPSS, and the LPSS, for each station across the CTMR, were calculated by equation (2)-(4). The SPSS, the EPSS, and the LPSS values differed among 26 stations. The average values of the SPSS, the EPSS, and the LPSS were 304th DOY, 82nd DOY, and 143 days, respectively. Figure 3 shows the spatial distribution of the SPSS, EPSS, and LPSS across the CTMR. Values of the SPSS were from the 260th to 323rd DOY (about September 16th to November 18th) and mainly after 293rd DOY (about October 19th). The EPSS was from the 54th to 134th DOY (February 23rd to May 13th) and mainly before 93rd DOY (April 2nd). The LPSS ranged from 97 to 239 days (about three months to eight months) and was shorter than 161 days in most of the region (Five months and 10 days). On average, the potential snowfall started October 29th, ended about March 20th, and lasted about 143 days across the CTMR. Spatially, the SPSS was smaller, the EPSS was larger, and the LPSS was longer in the north and center than in the south, especially in BYBLK and TEGT, where the LPSS was longer than seven months.

https://doi.org/10.5194/tc-2022-244
Preprint. Discussion started: 8 December 2022

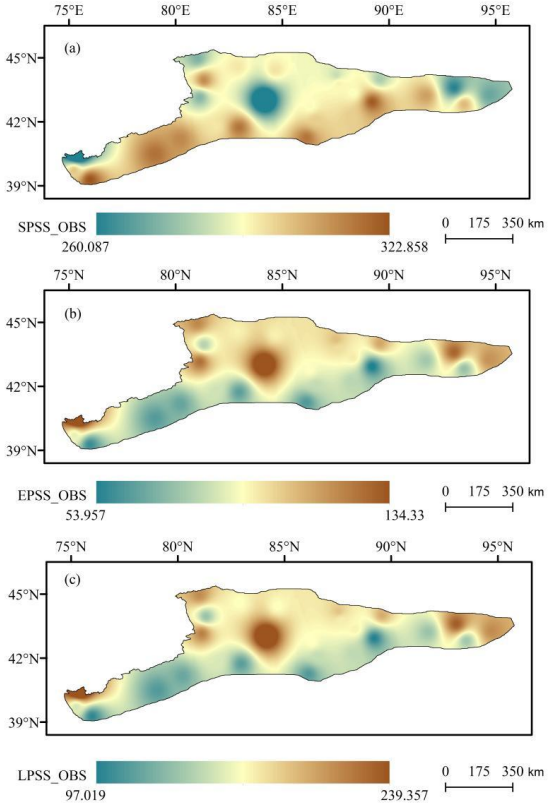

235 **Figure 3.** Spatial distribution of the average value of the SPSS (a), the EPSS (b), and the LPSS (c) in the CTMR.

3.2 Temporal variation of the PSP indicators in the past and present

All three indicators of the PSP experienced a clear changing trend during the study period. For both SPSS and EPSS, there were a significantly increasing trend and a significantly decreasing
240 trend at 0.05 confidence level during the last six decades, respectively (Figure 4a). Similar to the EPSS, a statistically significant decreasing trend was observed for the LPSS from 1962 to 2017/2020 (Figure 4b). The slopes of SPSS, EPSS, and LPSS were 1.1 days/10a, -1.6 days/10a, and -2.8 days/10a, respectively. That is, the potential snowfall season started later with 1.1 days per decade and ended earlier with 1.6 days per decade, and the duration of the potential snowfall
245 was shortened by 2.8 days per decade. In addition, the rate of advancing EPSS was faster than that of delaying SPSS.

https://doi.org/10.5194/tc-2022-244
Preprint. Discussion started: 8 December 2022

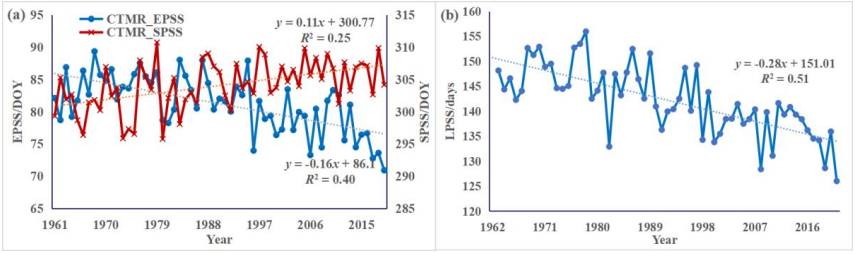

Figure 4. Annual time series and their trends of the SPSS and EPSS (a) during 1961-2020 and the LPSS (b) during 1962-2020 in the CTMR.

3.3 Spatial pattern of PSP indicators in the past and present

During 1961-2017/2020, in most of the region, the SPSS was with upward trends, the EPSS was with downward trends, and LPSS was with downward trends, respectively, implying that potential snowfall mostly started later, ended earlier and lasted shorter. Five stations, HM, KL, KQ, DBC, and KP, did not show a significantly changing trend for the SPSS. In KQ, BYBLK, and TLGT, there was no significant changing trend of the EPSS. For the LPSS, the non-significant changing trend was only found in KQ due to the non-significant changing trend of the SPSS and EPSS. The SPSS increased in most of the region, and the potential snowfall season started later for 2-13 days. The EPSS decreased across the area and the potential snowfall season ended earlier for 1-13 days. So the LPSS had been shortened by 1-27 days across the area (Figure 5). It would decrease annual total snowfall due to the reduction of snowfall days (Räisänen, 2016).

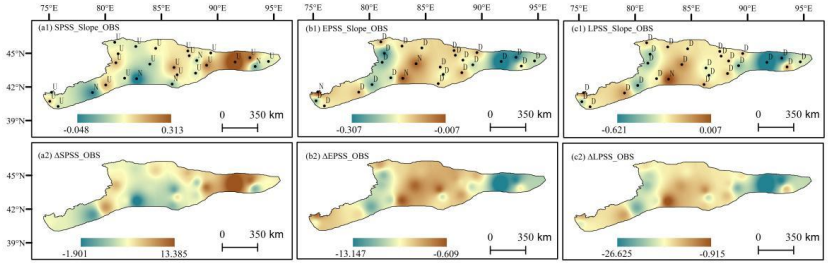

Figure 5. Changing trends and slopes of the SPSS (a1), EPSS (b1), and LPSS (c1) and their amplitude of variation (a2-c2) across the CTMR during 1961/1962-2017/2020. D for the downward trend, N for no trend, and U for the upward trend.

3.4 Temporal tendency of PSP indicators in the future

Figure 6 shows the time series of three PSP indicators in 2021-2100 and their average values during three periods (2021-2040, 2041-2070, and 2071-2100) under four different scenarios across the CTMR.

The SPSS will increase under all four scenarios from 2021 to 2100. And the upward slope of the SPSS increases from the SSP126 scenario to the SSP585 scenario (Figure 6a1). The average values of the SPSS will increase from 2021-2040 to 2071-2100 under all four scenarios. Significantly, the rise will be the steepest under the SSP585 scenario (Figure 6a2). Under the

https://doi.org/10.5194/tc-2022-244
Preprint. Discussion started: 8 December 2022

SSP585 scenario, the average value of the SPSS will reach 334th DOY during 2071-2100, indicating the potential snowfall season will start on November 28th in 2100.

The situation is different for the EPSS. The time series of the EPSS will initially remain at a certain level first and then increase under the SSP126 scenario. However, decreasing EPSS trends will occur under the other three scenarios, and values of the EPSS will decrease slightly from the SSP245 scenario to the SSP585 scenario (Figure 6b1). Average values of the EPSS will change less during the first two periods and increase slightly during 2071-2100 under the SSP126 scenario. Nevertheless, average values of the EPSS drop steeper and steeper in the three future periods under the SSP245 scenario to the SSP585 scenario (Figure 6b2). Under the SSP585 scenario, the average value of the EPSS will reach 63rd DOY during 2071-2100, implying that the potential snowfall season will end on March 3rd in 2100 across the CTMR under the SSP585 scenario.

The LPSS will go down in the coming 80 years under all four scenarios with a higher downward slope from the SSP126 scenario to the SSP585 scenario (Figure 6c1). Average values of the LPSS will decrease from 2021-2040 to 2071-2100 under all four scenarios. The drop will become sharper from the SSP126 scenario to the SSP585. The potential snowfall season will be shortened by up to 63 days in 2100 under the SSP585 scenario (Figure 6c2).

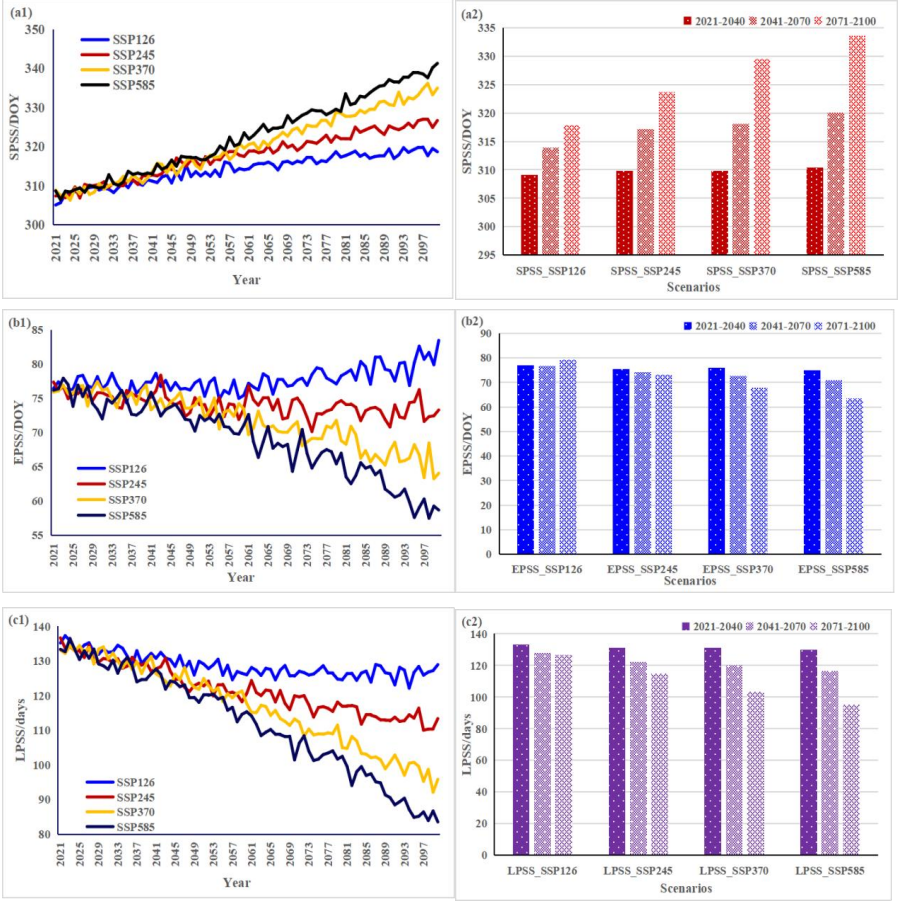

Figure 6. Time series of the SPSS (a1), the EPSS (b1), and the LPSS (c1) during 2021-2100 and their average

https://doi.org/10.5194/tc-2022-244
Preprint. Discussion started: 8 December 2022

values (a2-c2) during three periods (2021-2040, 2041-2070, and 2071-2100) under all four scenarios (SSP126, SSP245, SSP370, and SSP585) in the CTMR.

3.5 Spatial image of PSP indicators in the future

Figure 7 shows the spatial distribution of the SPSS, EPSS, and LPSS under four scenarios across the CTMR. Values of the SPSS will be 272nd-335th DOY (about September 27th to November 30th) under the SSP126 scenario, 275th-338th DOY (about October 1st to December 2nd) under the SSP245 scenario, 279th-341st DOY (about October 5th to November 5th) under the SSP370 scenario, and 283rd-344th DOY (about October 9th to December 10th) under the SSP585 scenario, respectively. The EPSS will happen 50th-135th DOY (February 19th to May 14th) under the SSP126 scenario, 48th-134th DOY (February 17th to May 13th) under the SSP245 scenario, 46th-130th DOY (February 15th to May 10th) under the SSP370 scenario, and 44th-125th DOY (February 13th to May 5th) under the SSP585 scenario, respectively. And the LPSS will last 81-229 days (two months and 20 days to seven months and 19 days) under the SSP126 scenario, 76-224 days (two months and 16 days to seven months and 14 days) under the SSP245 scenario, 71-217 days (two months and 11 days to seven months and seven days) under the SSP370 scenario, and 66-207 days (two months and six days to six months and 27 days) under the SSP585 scenario, respectively. Similar to the past and present, the SPSS will be smaller, the EPSS will be larger, and the LPSS will be longer in the north and center than in the south, especially in BYBLK and TEGT, where the LPSS will be longer than six months under all four scenarios.

During 2021-2100, the SPSS in the whole region will be with significant upward trends with gradually increasing rates (slopes) under the SSP126 scenario to the SSP585 scenario, which means potential snowfall season will start much later under the higher scenario in the coming 80 years. The amplitude of variation in the SPSS will increase with the enhancement of scenarios from the SSP126 to the SSP585. Under the SSP585 scenario, the SPSS will be delayed for 24-41 days. Spatially, the SPSS in the west and southwest will increase faster than that in the center and east, and it will delay the starting time of the potential snowfall season more days in the west and southwest under all four scenarios (Figure 8).

Under the SSP245, SSP370, and SSP585 scenarios, the EPSS shows significant downward trends with gradually increasing rates (slopes) in most of the region. While under the SSP126 scenario, the EPSS will be with significant upward trends at the rate from 0.2 day/10a to 1.1 day/10a across all the region. Therefore, the amplitude of variation in the EPSS will also be nonuniform under four future scenarios. Under the SSP126 scenario, the end of the potential snowfall season will be delayed for one to seven days across all the region, which will be brought forward up to 23 days under the SSP585 scenario. In the west and southwest of the CTMR, the EPSS will decrease faster, and the ending time will be in advance with more days under the SSP245, SSP370, and SSP585 scenarios (Figure 9).

Consequently, the LPSS shows significant downward trends with escalating rates from the SSP126 scenario to the SSP585 scenario. It will compress the length of the potential snowfall season by 4-10 days under the SSP126 scenario, 11-31 days under the SSP245 scenario, 23-45 days under the SSP370 scenario, and 32-63 days under the SSP585 scenario. In the west and southwest of the CTMR, the LPSS will be cut down by more days under all four scenarios (Figure 10).

In summary, the SPSS will increase significantly with the scenario increase from the SSP126 to

https://doi.org/10.5194/tc-2022-244
Preprint. Discussion started: 8 December 2022

the SSP585, but, at the same time, the EPSS and LPSS will decrease considerably. It will delay the start of the potential snowfall season for 24-41 days under the SSP585 scenario, whilst the end of the potential snowfall season will be 1-7 days delayed under the SSP126 scenario and up to 23 days in advance under the SSP585 scenario. As a result, the length of the potential snowfall season will be cut down by 32-63 days under the SSP585 scenario. Spatially, in the west and southwest of the CTMR, the starting time, ending time, and length of the potential snowfall season will be change faster than other places.

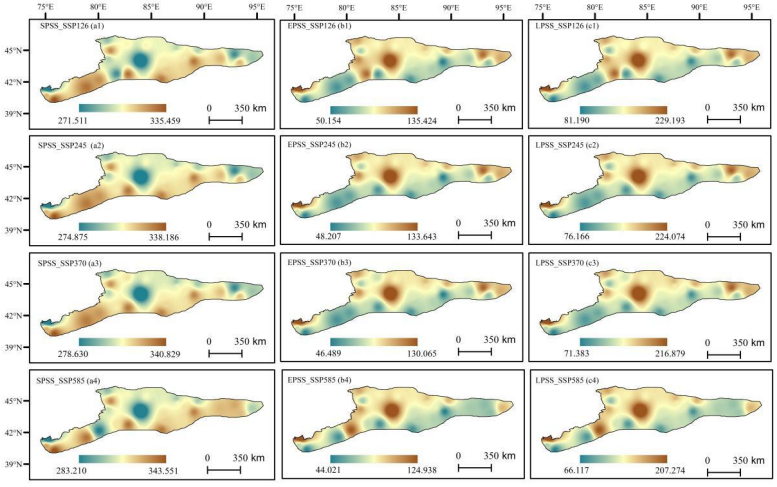

Figure 7. Spatial distribution of the average value of the SPSS (a1-a4), EPSS (b1-b4), and LPSS (c1-c4) under four different scenarios (SSP126, SSP245, SSP370, and SSP585) across the CTMR during 2021-2100.

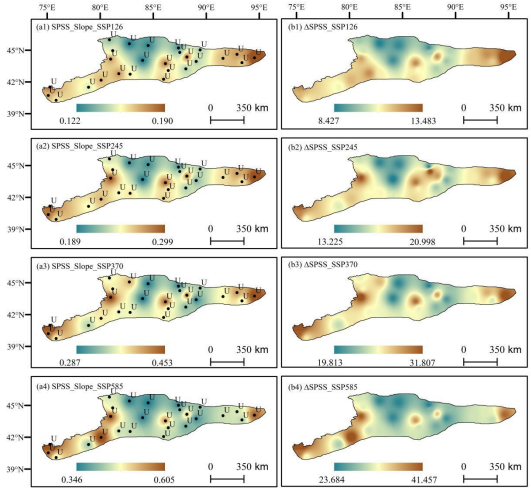

Figure 8. Changing trends and slopes of the SPSS under the SSP126 (a1), SSP245(a2), SSP370 (a3), and SSP585(a4) scenarios and its amplification (b1-b4) across the CTMR during 2021-2100. D for the downward trend, N for no trend, and U for the upward trend

https://doi.org/10.5194/tc-2022-244
Preprint. Discussion started: 8 December 2022

The Cryosphere
Discussions
Open Access
EGU

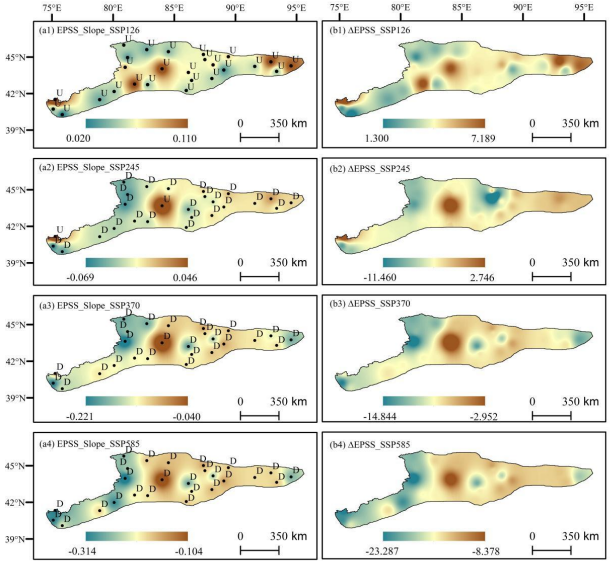

Figure 9. Changing trends and slopes of the EPSS under the SSP126 (a1), SSP245(a2), SSP370 (a3), and SSP585(a4) scenarios and its amplification (b1-b4) across the CTMR during 2021-2100. D for the downward trend, N for no trend, and U for the upward trend.

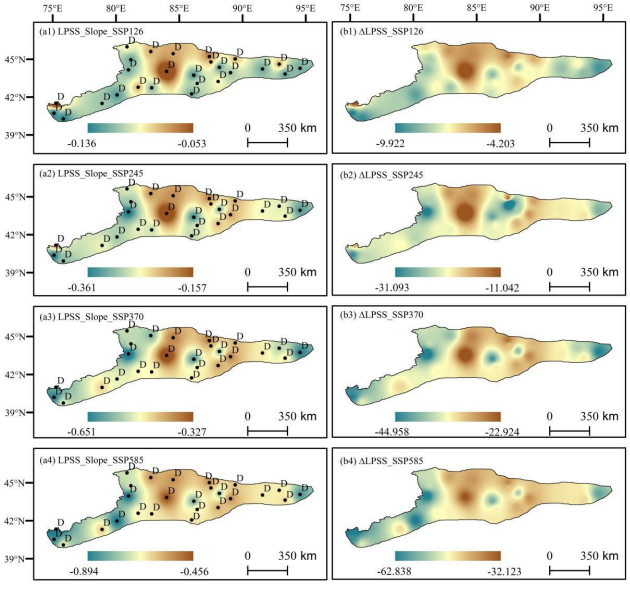

Figure 10. Changing trends and slopes of the LPSS under the SSP126 (a1), SSP245(a2), SSP370 (a3), and SSP585(a4) scenarios and its amplification (b1-b4) across the CTMR during 2021-2100. D for the downward trend, N for no trend, and U for the upward trend.

https://doi.org/10.5194/tc-2022-244
Preprint. Discussion started: 8 December 2022

4 Discussion

4.1 Performance of PSP indicators

Much previous work focused on variability, trends, spatial-temporal pattern, extremes, and events of snowfall over the snow-dominated regions in the world (Baijnath-Rodino et al., 2018; Nazzareno et al., 2019; Bai et al., 2019; Takahashi et al., 2021; Lin and Chen, 2022). Less attention was paid to the change in phenology of potential snowfall. Therefore, the SPSS, EPSS, and LPSS, were presented skillfully based on the semi-sinusoidal curve of daily air temperature combined with various rain-snow thresholds. The SPSS and EPSS represent the start and end of the potential snowfall season within a year. The length of the potential snowfall season, LPSS, equals the difference value between the EPSS in the second year and the SPSS in that same year. Our work showed the potential snowfall season was mainly from October 14th to April 7th across the CTMR. In comparison, the observed snowfall season was from November to March in the CTMR (Tian et al., 2020). Thus, the consistency between the observed and the potential snowfall season was high, and the potential snowfall season could cover the observed one. It proved that the SPSS, EPSS, and LPSS reproduced the feature of potential snowfall phenology across the CTMR well and could be expanded to other snow-dominated regions worldwide.

4.2 Spatial and temporal heterogeneity

The tendency in PSP indicators showed relative continuity from past and present to future. During both the historical period (1961-2020) and the future period (2021-2100), the time series of SPSS and LPSS presented a uniform upward or downward trend, although the observed SPSS and LPSS fluctuated more sharply (Figure 11a and 11c). The exception happened in that of the EPSS. The changing trends of the observed EPSS were consistent with that of the projected one under SSP245, SSP370, and SSP585 scenarios, but opposite to that of the projected one under SSP126 scenario (Figure 11b). In addition, different from the historical period, the rate of postponing SPSS was faster than that of advancing EPSS under all four scenarios. It may be caused by seasonal diversity in the warming rate of air temperature. The amplitude of air temperature variation under all four scenarios will be more significant in autumn and winter than in the other two seasons (Figure 12). The higher emission scenario will bring a higher rate of climate warming, which leads to the advancing SPSS and postponing EPSS. As a result, the reduction of LPSS will speed up from the historical period to the SSP585 scenarios in the future (Table 3).

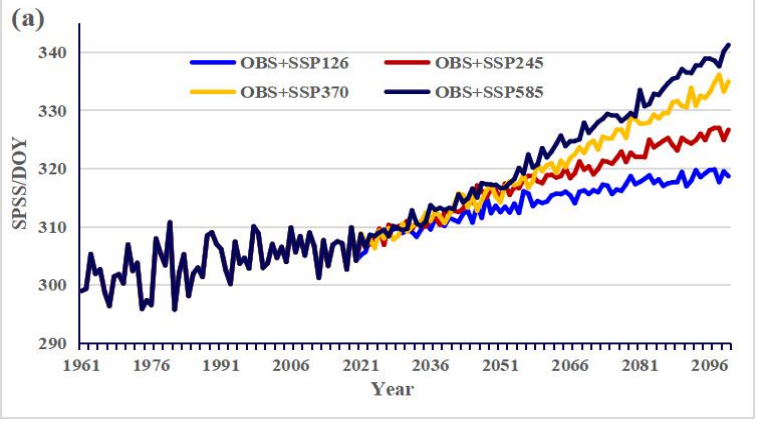

https://doi.org/10.5194/tc-2022-244
Preprint. Discussion started: 8 December 2022

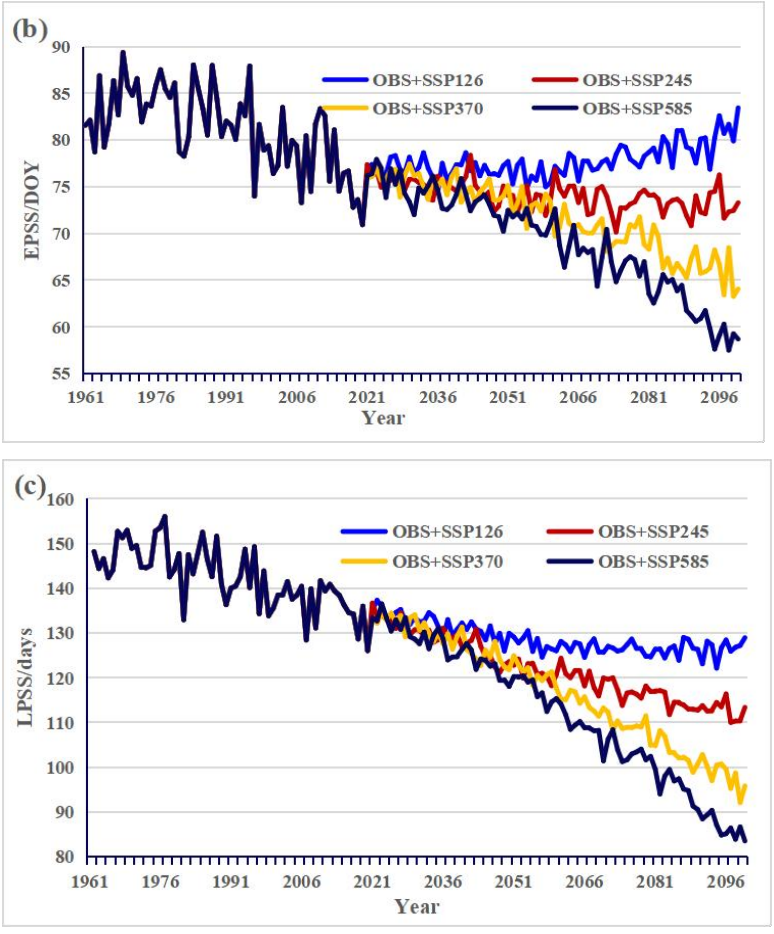

395 **Figure 11.** Time series of the SPSS (a), EPSS (b), and LPSS (c) from 1961 to 2100 in the CTMR. OBS means time series base on observation data during 1961-2020; SSP126, SSP245, SSP370, and SSP585 refer to time series base on CIMP6 data during 2021-2100.

Table 3. The changing rate in PSP indicators in the CTMR

	SPSS	EPSS	LPSS
OBS	1.15/10a	-1.56/10a	-2.66/10a
SSP126	1.54/10a	0.44/10a	-1.14/10a
SSP245	2.45/10a	-0.40/10a	-2.87/10a
SSP370	3.60/10a	-1.50/10a	-5.06/10a
SSP585	4.30/10a	-2.21/10a	-6.46/10a

400

https://doi.org/10.5194/tc-2022-244
Preprint. Discussion started: 8 December 2022

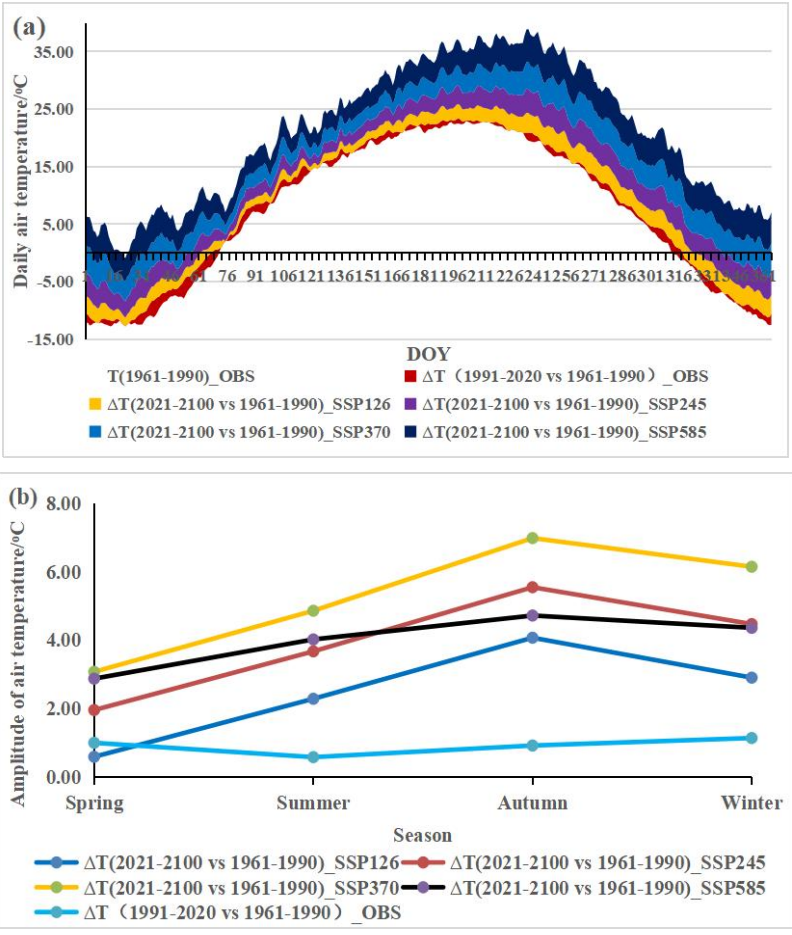

Figure 12. The intra-annual amplitude of daily air temperature variation (a) and its seasonal diversity (b) in the CTMR. T(1961-1990)_OBS is the observed mean daily air temperature during 1961-1990; ΔT(1991-2020 vs. 1961-1990)_OBS is the amplitude of air temperature variation during 1991-2020 compared that during 1961-1990; ΔT(2021-2100 vs. 1961-1990)_SSP126 means the amplitude of air temperature variation during 2021-2100 under the SSP126 scenario comparing that during 1961-1990; the same to ΔT(2021-2100 vs. 1961-1990)_SSP245, ΔT(2021-2100 vs. 1961-1990)_SSP370, and ΔT(2021-2100 vs. 1961-1990)_SSP585.

4.3 Uncertainty

Although CMIP6 data could capture surface air temperature trends well (Fan et al., 2020), it could not reproduce seasonal diversity with the same good performance. The correlation between the observed and the simulated values from CMIP6 during 1961-2020 varied from 0.93 to 0.98 (Figure 13a). The air temperature was underestimated by 0.26 ℃ in spring and overestimated slightly in the other three seasons (Figure 13b). It may lead to the overestimation of the SPSS and the underestimation of the EPSS under four different scenarios. In addition, uncertainty may come from selected data. Data from the 14 models selected may not eliminate modeling errors. Further research could consider data from more CMIP6 models.

https://doi.org/10.5194/tc-2022-244
Preprint. Discussion started: 8 December 2022

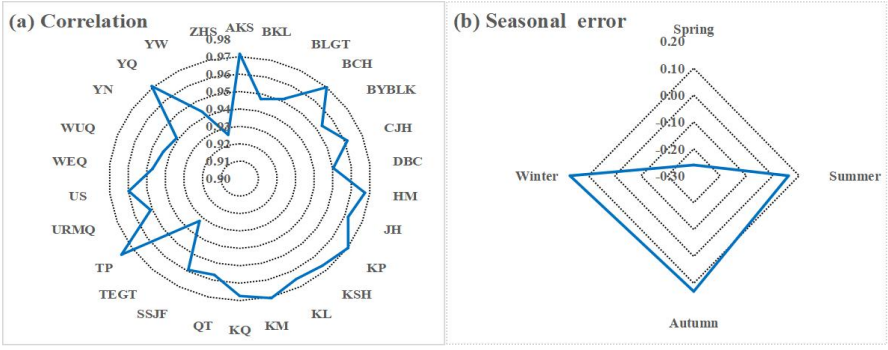

Figure 13. Correlation between the observed and CMIP6 at meteorological station scale (a) and its seasonal mean error (b) across the CTMR.

5 Conclusions

In this study, we initially defined three indicators of the potential snowfall penology (the SPSS, EPSS, and LPSS) and analyzed their spatial-temporal variation in the past, present, and future over the CTMR. This research indicated three indicators reproduced the feature of potential snowfall phenology across the CTMR well and could be recommended to other snow-dominated regions worldwide.

Potential snowfall season started on about October 29th, ended on about March 20th, and lasted about 143 days across the CTMR on average during 1961-2017/2020. It found significant delaying in the starting time, advancing in the ending time, and reduction in the duration of the potential snowfall season, respectively. The potential snowfall season started later for 2-13 days at a rate of 1.1 days per decade and ended earlier for 1-13 days at a rate of 1.6 days per decade with a shorter potential snowfall duration for 1-27 days at the rate of 2.8 days per decade across all the region. The potential snowfall season started later, ended later, and lasted longer in the north and center than in the south, especially in BYBLK and TEGT, where the potential snowfall season was longer than seven months.

The starting time, ending time, and duration of the potential snowfall season will vary under four scenarios during 2021-2100. The potential snowfall season will start much later, end earlier, and last less time under the higher emission scenario in the coming 80 years. The starting time will be postponed with gradually upward slopes under the scenarios from SSP126 to SSP585. Under the SSP585 scenario, the potential snowfall season will be from about October 9th to December 10th. Ending time under the SSP126 scenario showed opposite changing trends from that under the SSP245 scenario to the SSP585 scenario. It will change less during 2021-2070 and be postponed slightly during 2071-2100 under the SSP126 scenario. Under the SSP585 scenario, the potential snowfall season will end on February 13th to May 5th across the CTMR. The length will gradually decrease from the SSP126 scenario to the SSP585 scenario in the coming 80 years. The duration of the potential snowfall season will be shortened up to 63 days in 2100 under the SSP585 scenario. In the west and southwest of the CTMR, the length of the potential snowfall season will be cut down by more days because of the more starting time delayed and ending time advanced under all four scenarios.

Spatial and temporal heterogeneity existed across the CTMR for the seasonal diversity of

https://doi.org/10.5194/tc-2022-244
Preprint. Discussion started: 8 December 2022

warming. Uncertainty is also inevitable because of the quantity and quality of data selected. Further research may focus on selecting multivariate data and applying our indicators of potential snowfall penology in the broader region.

Code/Data Availability. Data are available upon reasonable request to the corresponding author.

Author contributions. Xuemei Li wrote and organized the main text; Xinyu Liu processed data about historical and future temperature data; Kaixin Zhao provided figures; Other group members offered further insight, comments, and editorial suggestions.

Competing interests. The authors declare that they have no conflict of interest.

Acknowledgements. This work was financially supported by the National Natural Sciences Foundation of China (42261026, 41971094, 42161025, and 42101096), Higher Education Innovation Foundation of Education Department of Gansu Province (2022A-041), and the Foundation of A Hundred Youth Talents Training Program of Lanzhou Jiaotong University.

References

Aizen, V. B., Aizen, E. M., Melack, J. M., and Dozier, J.: Climatic and hydrologic changes in the Tien Shan, central Asia, J. Climate, 10, 1393–1404, https://doi.org/10.1175/1520-0442(1997)010<1393:CAHCIT>2.0.CO;2, 1997.

Bai, L., Shi, C., Shi, Q., Li, L., Wu J., Yang, Y., Sun, S., Zhang, F.: Change in the spatiotemporal pattern of snowfall during the cold season under climate change in a snow-dominated region of China, Int. J. Climatol., 39, 5702–5719, https://doi.org/10.1002/joc.6182, 2019.

Baijnath-Rodino, J. A., Duguay, C. R., Ledrew, E.: Climatological trends of snowfall over the Laurentian Great Lakes Basin, Int. J. Climatol., 38, 3942–3962, https://doi.org/10.1002/joc.5546, 2018.

Clow, D.W.: Changes in the timing of snowmelt and streamflow in Colorado: A response to recent warming, J. Clim., 23, 2293–2306, https://doi.org/10.1175/2009JCLI2951.1, 2010.

Daloz, A. S., Mateling, M., L'Ecuyer, T., Kulie, M., Wood, N. B., Durand, M., Wrzesien, M., Stjern, C. W., and Dimri, A. P.: How much snow falls in the world's mountains? A first look at mountain snowfall estimates in A-train observations and reanalyses, The Cryosphere, 14, 3195–3207, https://doi.org/10.5194/tc-14-3195-2020, 2020.

Dedieu, J. P., Lessard-Fontaine, A., Ravazzani, G., Cremonese, E., Shalpykova, G., Beniston, M.: Shifting mountain snow patterns in a changing climate from remote sensing retrieval, Sci. Total. Environ., 493, 1267–1279, https://doi.org/10.1016/j.scitotenv.2014.04.078, 2014.

Fan, X., Duan, Q., Shen, C., Wu, Y. and Xing C.: Global surface air temperatures in CMIP6: historical performance and future changes, Environ. Res. Lett., 15, 104056, https://doi.org/10.1088/1748-9326/abb051, 2020.

Gao, L., Deng, H., Lei, X., Wei, J., Chen, Y., Li, Z., Ma, M., Chen, X., Chen, Y., Liu, M., and Gao, J.: Evidence of elevation-dependent warming from the Chinese Tian Shan, The Cryosphere, 15, 5765–5783, https://doi.org/10.5194/tc-15-5765-2021, 2021.

Guo, L., Li, L.: Variation of the proportion of precipitation occurring as snow in the Tian Shan Mountains, China, Int. J. Climatol., 35, 1379–1393, https://doi.org/10.1002/joc.4063, 2015.

https://doi.org/10.5194/tc-2022-244
Preprint. Discussion started: 8 December 2022

Hamlet, A. F., Mote, P. W., Clark, M. P., and Lettenmaier, D. P.: Effects of temperature and precipitation variability on snowpack trends in the western United States, J. Clim., 18, 4545–4561, https://doi.org/10.1175/JCLI3538.1, 2005.

Han, W., Xiao, C., Dou, T., Ding, M.: Changes in the proportion of precipitation occurring as rain in Northern Canada during spring–summer from 1979–2015, Adv. Atmos. Sci., 35, 1129–1136, https://doi.org/10.1007/s00376-018-7226-3, 2018.

Hock, R., Roberts, C., Masson-Delmotte, V.: "High mountain areas" in IPCC Special Report on the Ocean and Cryosphere in a Changing Climate, Cambridge Univ. Press, 131–202, 2022.

Hu, R., J.: Physical Geography of the Tianshan Mountains in China, China Environmental Science Press, Beijing, 139–142, 2004 (in Chinese).

Immerzeel, W. W., Lutz, A. F., Andrade, M., Bahl, A., Biemans, H., Bolch, T., Hyde, S., Brumby, S., Davies, B. J., Elmore, A. C., Emmer, A., Feng, M., Fernández, A., Haritashya, U., Kargel, J. S., Koppes, M., Kraaijenbrink, P. D. A., Kulkarni, A. V., Mayewski, P. A., Nepal, S., Pacheco, P., Painter, T. H., Pellicciotti, F., Rajaram, H., Rupper, S., Sinisalo, A., Shrestha, A. B., Viviroli, D., Wada, Y., Xiao, C., Yao, T., and Baillie, J. E. M.: Importance and vulnerability of the world's water towers, Nature, 577, 364–369, https://doi.org/10.1038/s41586-019-1822-y, 2020.

Jennings, K. S., Winchell, T. S., Livneh, B., Molotch N. P.: Spatial variation of the rain–snow temperature threshold across the Northern Hemisphere, Nat. Commun., 9, 1–9, https://doi.org/10.1038/s41467-018-03629-7, 2018.

Jiang, F., Li, X., Wei, B., Hu, R., and Li, Z.: Observed trends of heating and cooling degree-days in Xinjiang province, China, Theor. Appl. Climatol., 97, 349–360, https://doi.org/10.1007/s00704-008-0078-5, 2009.

Kapnick, S. B., Delworth, T. L., Ashfaq, M., Malyshev, S., and Milly, P. C. D.: Snowfall less sensitive to warming in Karakoram than in Himalayas due to a unique seasonal cycle, Nat. Geosci., 7, 834–840, https://doi.org/10.1038/ngeo2269, 2014.

Kappelle, M.: WMO Statement on the State of the Global Climate in 2019, 2020.

Kendall, M. G.: Rank correlation methods, Brit. J. Psychol., 25, 86–91, 1990.

Krasting, J. P.: Variations in Northern Hemisphere snowfall: an analysis of historical trends and the projected response to anthropogenic forcing in the twenty-first century, Doctor of Philosophy, Rutgers, The State University of New Jersey, 2008.

Li, X., Gao, P., Li, Q., Tang, H.: Muti-paths Impact from Climate Change on Snow Cover in Tianshan Mountainous Area of China. Adv. Clim. Chang. Res., 12, 303–312, https://doi.org/10.12006/j.issn.1673-1719.2015.184, 2016 (in Chinese with English abstract).

Li, X., Jiang, F., Li, L., Wang, G.: Spatial and temporal variability of precipitation concentration index, concentration degree and concentration period in Xinjiang province, China, Int. J. Climatol., 31, 1679–1693, https://doi.org/10.1002/joc.2181, 2011.

Li, X., Li, L., Yuan, S., Yan, H., and Wang, G.: Temporal and spatial variation of 10-day mean air temperature in Northwestern China. Theor. Appl. Climatol., 119, 285–298, https://doi.org/10.1007/s00704-014-1100-8, 2015.

Li, X., Simonovic, S. P., Li, L., Zhang X., and Qin Q.: Performance and uncertainty analysis of a short-term climate reconstruction based on multi-source data in the Tianshan Mountains region, China, J. Arid Land, 12, 374–396, https://doi.org/10.1007/s40333-020-0065-y, 2020.

Li, X., Zhang, B., Ren, R., Li, L., and Simonovic, S. P.: Spatio-temporal Heterogeneity of Climate Warming in the Chinese Tianshan Mountainous Region, Water, 14, 199,

https://doi.org/10.3390/w14020199, 2022.

Li, X.: Climate change and its impact in the Chinese Tianshan mountainous region, Publishing House of Electronics Industry, 2021 (in Chinese).

Li, Y., Chen, Y., Li, Z.: Climate and topographic controls on snow phenology dynamics in the Tienshan Mountains, Central Asia, Atmos. Res., 236, 104813, https://doi.org/10.1016/j.atmosres.2019.104813, 2020.

Lin, W., Chen, H.: Changes in the spatial-temporal characteristics of daily snowfall events over the Eurasian continent from 1980 to 2019, Int. J. Climatol., 42, 1841–1853, https://doi.org/10.1002/joc.7339, 2022.

Loth, B., Graf, H. F., Oberhuber, J. M.: Snow cover model for global climate simulations, J. Geophys. Res.-Atmos., 98, 10451–10464, https://doi.org/10.1029/93JD00324, 1993.

Marshall, J., Plumb, R. A.: Atmosphere, ocean, and climate dynamics: an introductory text, Chapter 2: The global energy balance, 9–22, 2008.

Masson-Delmotte, V., Zhai, P., Pirani, A., Connors, S. L., Péan, C., Chen, Y., Goldfarb, L., Gomis, M. I., Matthews, J. B. R., Berger, S., Huang, M., Yelekçi, O., Yu, R., Zhou B., Lonnoy, E., Maycock, T. K., Waterfield, T., Leitzell, K., Caud, N.: IPCC,2021: In Climate Change 2021: The Physical Science Basis. Contribution of working group I to the sixth assessment report of the intergovernmental panel on climate change, Cambridge University Press, Cambridge, United Kingdom and New York, NY, USA, in press, 2021.

McAfee, S., Walsh, J., Rupp, S.: Statistically downscaled projections of snow/rain partitioning for Alaska, Hydrol. Process., 28, 3930–3946, https://doi.org/10.1002/hyp.9934, 2014.

McCabe, G. J., Wolock, D. M.: Recent declines in western U.S. snowpack in the context of twentieth-century climate variability, Earth Interact., 13, 1–15, https://doi.org/10.1175/2009EI283.1, 2009.

Mote, P. W., Hamlet, A. F., Clark, M. P., and Lettenmaier, D. P.: Declining mountain snowpack in western North America, B. Am. Meteorol. Soc., 86, 39–50, https://doi.org/10.1175/BAMS-86-1-39, 2005.

Nazzareno, D., Büntgen, Ulf, Gianni, B.: Mediterranean winter snowfall variability over the past millennium, Int. J. Climatol., 39, 384–394. https://doi.org/10.1002/joc.5814, 2019.

O'Neill, B. C., Tebaldi, C., Van, Vuuren, D. P., Eyring, V., Friedlingstein, P., Hurtt, G., Knutti, R., Kriegler, E., Lamarque, J., Lowe, J., Meehl, G. A., Moss, R., Riahi, K., and Sanderson, B. M.: The scenario model intercomparison project (ScenarioMIP) for CMIP6, Geosci. Model Dev., 9, 3461–3482, https://doi.org/10.5194/gmd-9-3461-2016, 2016.

Piazza, M., Boé, J., Terray, L., Pagé, C., Sanchez-Gomez, E., and Déqué, M.: Projected 21st century snowfall changes over the French Alps and related uncertainties, Climatic Change, 122, 583–594, https://doi.org/10.1007/s10584-013-1017-8, 2014.

Raisanen, J.: Twenty-first century changes in snowfall climate in Northern Europe in ENSEMBLES regional climate models, Clim. Dyn., 46, 339–353, https://doi.org/10.1007/s00382-015-2587-0, 2016.

Ren, R., Li, X., Li, L., Qin, Q., Huang, Y.: Discrimination of driving factors of precipitation forms in Tianshan Mountains area of China, J. Arid Land Res. and Environ., 34, 112–117, 2020 (in Chinese with English abstract).

Ren, R., Li, X., Li, Z., Li, L., and Huang, Y.: Projected change in precipitation forms in the Chinese Tianshan Mountains based on the Back Propagation Neural Network Model, J. Mt. Sci.,

19, 689–703, https://doi.org/10.1007/s11629-021-7076-9, 2022.

Roux, E. L., Evin, G., Eckert, N., Blanchet, J., and Morin, S.: Elevation-dependent trends in extreme snowfall in the french alps from 1959 to 2019, The Cryosphere, 15, 4335–4356, https://tc.copernicus.org/articles/15/4335/2021/, 2021

Sabine, B. R., Mathieu, G., Olivier, B., Miska, L., Carmen, C., Gregoire, M., Antoine, G.: From white to green: Snow cover loss and increased vegetation productivity in the European Alps, Science, 376, 1119–1122, https://doi.org/10.1126/science.abn6697, 2022.

Sorg, A., Bolch, T., Stoffel, M., Solomina, O. N., and Beniston, M.: Climate change impacts on glaciers and runoff in Tien Shan (Central Asia), Nat. Clim. Change, 2, 725–731, https://doi.org/10.1038/nclimate1592, 2012.

Sun, F., Hall, A., Schwartz, M., Walton, D. B., and Berg, N.: Twenty-First-Century Snowfall and Snowpack Changes over the Southern California Mountains, J. Climate, 29, 91–110, https://doi.org/10.1175/JCLI-D-15-0199.1, 2016.

Takahashi, H. G.: Long-term trends in snowfall characteristics and extremes in Japan from 1961 to 2012, Int. J. Climatol., 41, 2316–2329, https://doi.org/10.1002/joc.6960, 2021.

Tamang, S. K., Ebtehaj, A. M., Prein, A. F., and Heymsifield, A. J.: Linking global changes of snowfall and wet-bulb temperature, J. Climate, 33, 39–59, https://doi.org/10.1175/JCLI-D-19-0254.1, 2020.

Tian, Y., Li, X., Li, Z., Qin, Q.: Spatial and temporal variations of different precipitation types in the Tianshan Mountains from 1850-2017, Arid Land Geogr., 43, 308–318, 2020 (in Chinese with English abstract).

Yang, J., Fang, G., Chen, Y., and De-Maeyer, P.: Climate change in the Tianshan and northern Kunlun Mountains based on GCM simulation ensemble with Bayesian model averaging, J. Arid Land, 9, 622–634, https://doi.org/10.1007/s40333-017-0100-9, 2017.

Yang, T., Li, Q., Ahmad, S., Zhou, H., and Li, L.: Changes in Snow Phenology from 1979 to 2016 over the Tianshan Mountains, Central Asia, Remote Sens., 11, 499. https://doi.org/10.3390/rs11050499, 2019.

Yang, T., Li, Q., Hamdi, R., Zou, Q., Chen, X., Maeyer, P., Cui, F., Li, L.: Snowfall climatology in the Tianshan Mountains based on 36 cold seasons of WRF dynamical downscaling simulation, Atmos. Res., 270, 106057, https://doi.org/10.1016/j.atmosres.2022.106057, 2022.

Zhang, L., Chen, X., Xin, X.: Short commentary on CMIP6 Scenario Model Intercomparison Project (ScenarioMIP), Clim. Chang. Res., 15, 519–525, https://doi.org/10.12006/j.issn.1673-1719.2019.082, 2019.

Zhang, X., Li, X., Gao, P., Li, Q., and Tang, H.: Separation of precipitation forms based on different methods in Tianshan Mountainous Area, Northwest China, J. Glaciol. Geocryol., 39, 235–244, 2017 (in Chinese with English abstract).

Zhang, X., Li, X., Li, L., Zhang S., and Qin, Q.: Environmental factors influencing snowfall and snowfall prediction in the Tianshan Mountains, Northwest China, J. Arid Land, 11, 15–28, https://doi.org/10.1007/s40333-018-0110-2, 2019.